# Phase Formation Study of Ca-Terephthalate MOF-Type Materials

**ARTICLE** *in* CRYSTAL GROWTH & DESIGN · FEBRUARY 2015

Impact Factor: 4.89 · DOI: 10.1021/cg501273b



**2 AUTHORS:**

Matjaz Mazaj

National Institute of Chemistry

**51** PUBLICATIONS **427** CITATIONS

SEE PROFILE

Natasa Zabukovec Logar

National Institute of Chemistry

**74** PUBLICATIONS **746** CITATIONS

SEE PROFILE

CRYSTAL GROWTH & DESIGN

Article

pubs.acs.org/crystal

# Phase Formation Study of Ca-Terephthalate MOF-Type Materials

Matjaž Mazaj*,† and Nataša Zabukovec Logar†

National Institute of Chemistry, Hajdrihova 19, 1001 Ljubljana, Slovenia

Supporting Information

**ABSTRACT:** Ca(BDC)(DMF)($H_2O$) with square lattice topology (sql) and rhombic-shaped channels crystallizes under solvothermal conditions ($H_2O$/DMF mixture) in orthorhombic (Ca-BDC-*orth*) and triclinic (Ca-BDC-*tric*) conformations. The latter structure is solved and described here for the first time. The main difference between the two phases lies in the orientation of the coordinated DMF molecule located within the channels of the structure, influencing their porosity properties. In spite of the small deviances in crystal structure, the formation of individual phases can be controlled by the amount of base agent (TEA) and the temperature of crystallization. Triclinic phase is formed at lower synthesis temperature, and it is transformed into orthorhombic phase at increased temperatures. Systematic phase formation study varying TEA/$Ca^{2+}$ molar ratios and the synthesis temperature showed that higher temperature of the synthesis is required for the Ca-BDC-*orth* phase to occur from Ca-BDC-*tric* using the TEA/$Ca^{2+}$ ratio between 0.63−1.30 compared to the syntheses with TEA/$Ca^{2+}$ values out of this range. Within the range of 0.63−1.30 the dissociation of the base is in the buffer region indicating that stability of triclinic phase is related to the thermodynamics at equilibrium conditions.

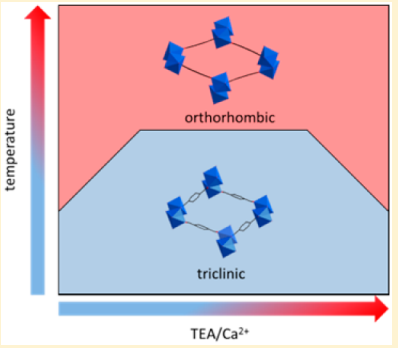


## INTRODUCTION

Metal−organic frameworks (MOFs) are built from inorganic building units connected through organic ligands into the porous structures. Possibility to design MOFs with targeted properties and ability to functionalize frameworks by post-modification processes enable their potential implementation in various fields such as gas sorption, catalysis, optics, sensors, biotechnology, etc.[1−22] In spite of rapidly growing interest for MOFs applications, their crystallization mechanisms are less investigated and are relatively unknown for most of the systems. The formation of MOF phase often depends on many synthesis parameters that influence the thermodynamics and kinetics of crystallization process. This makes the determination of crystallization mechanisms difficult. They are usually specific for a particular system and cannot be generalized.

Among many variables, the type of solvent used in the synthesis turned out to be one of the most important parameters governing the coordination process of MOF structures.[23−26] Furthermore, the synthesis procedures often involve cosolvents, which can have a templating role or ligand role[27−31] or they can directly influence the structure formation by affecting the solubility of the precursors, the polarity, ionic strength, boiling points, and autogenous pressures and thus govern the overall kinetics of the crystallization process.[24,32−34] Particularly, the organic bases (amines) used as cosolvents were found to have an important role on the MOFs formation, both as structure directing agents or as coordinating ligands.[35−38] Amines with accessible N-donor sites are usually relatively strongly bonded to the MOF frameworks; thus, the emptying of the pores is hindered due to the difficulties of the template removal. Therefore, for the formation of porous structures with permanent porosities, the use of trialkylamines representing strong base agents with ability for O-donor ligand deprotonation and at the same time poor affinity for binding to metal sites seem to be more appropriate.[39−45]

The investigations of crystallization processes, including the solvent and the cosolvent roles, are mostly performed on the transition-metal based MOFs and rarely on structures based on s-block metals (Mg- and Ca-MOFs in particular).[33,45−48] Latter are, however, advantageous in possible implementations in bioapplications and gas storage due to their nontoxicity and light weight. We already investigated the structural dynamics of Ca-terephthalate structure upon heating and hydration/dehydration processes.[49] Its framework with chemical formula Ca(BDC)(DMF)($H_2O$) possesses 44 net topology with rhombic-shaped channels and exists in two conformations (orthorhombic and triclinic).[50] In this contribution we deal with the detailed formation studies of the two Ca-terephthalate phases and discuss the impact of the base agents on the crystallization dynamics.

## EXPERIMENTAL SECTION

**General Characterization Methods.** X-ray powder diffraction data of the as-synthesized products were collected on a PANalytical X'Pert PRO high-resolution diffractometer with CuK$\alpha$1 radiation ($\lambda$ = 1.5406 Å) in the range from 5 to 35° 2$\theta$ with the step of 0.016° per 100 s using fully opened 100 channel X'Celerator detector. For the purpose of the structure determination of Ca-BDC-tric phase, the XRD pattern was collected using wider 2$\theta$ range (from 5 to 90°) and step of 0.008° per 300 s. XRD pattern was indexed with DICVOL06 package[51] for the first 20 lines. The crystal structure was solved in

Received: August 26, 2014
Revised: December 17, 2014
Published: December 19, 2014





DOI: 10.1021/cg501273b
Cryst. Growth Des. 2015, 15, 617−624

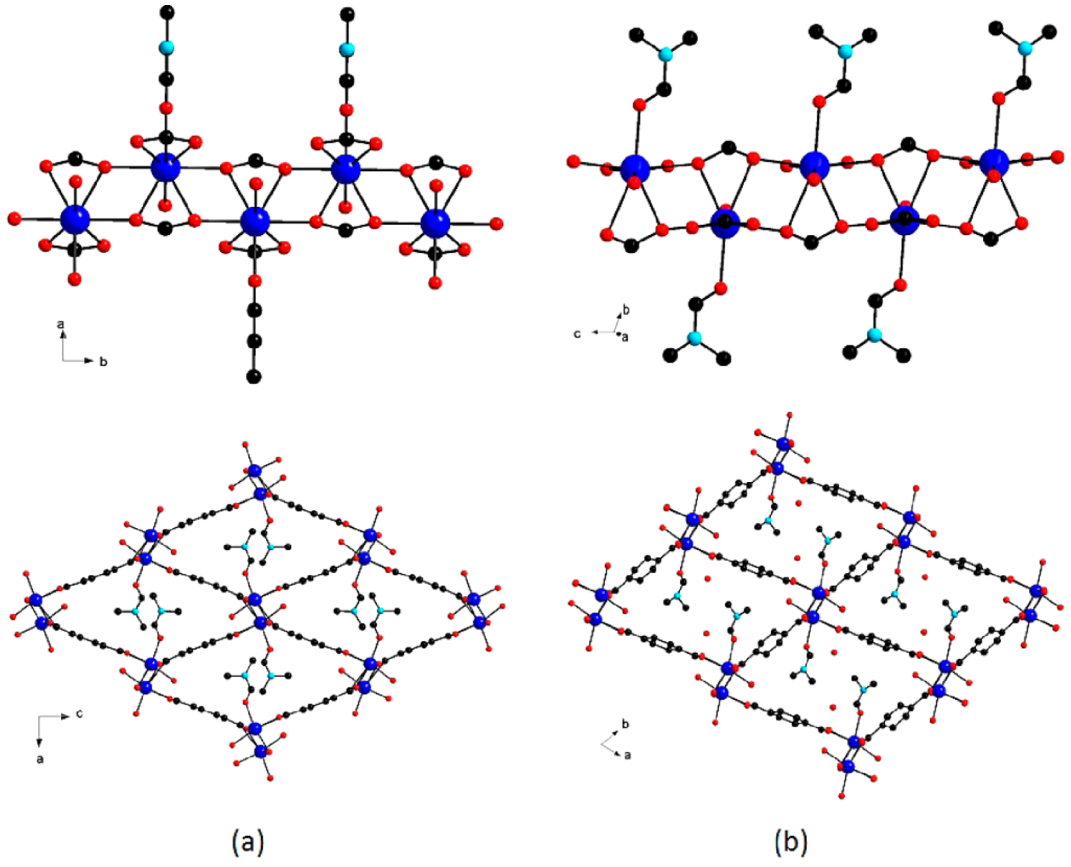


**Figure 1.** Ball and stick structure presentations of (a) Ca-BDC-*orth* and (b) Ca-BDC-*tric* phases. Upper schemes represent $CaO_8$ chains with the coordinated DMF molecules; lower ones show the view of the structures along the channel directions. Ca-BDC-*tric* structure also shows partially occupied O atoms belonging to adsorbed water molecules. H atoms are omitted for clarity. Dark blue circles, Ca atoms; red circles, O atoms; black circles, C atoms; light blue circles, N atoms.

triclinic $P\bar{1}$ (No. 2) symmetry with the parameters of $a$ = 12.4530(1) Å, $b$ = 10.2066(1) Å, $c$ = 6.7002(1) Å, $\alpha$ = 107.468(1)°, $\beta$ = 104.433(1)°, and $\gamma$ = 66.7620(8)°. Whole pattern profile refinement without structural parameters using LeBail method[52] confirmed the adequacy of the unit cell. Structure determination was performed by using EXPO2009 package.[53] The first electron density map revealed positions of all Ca and O atoms, whereas all C atoms were located by the difference Fourier map analysis. Hydrogen atoms were located geometrically. The obtained model was refined by Rietveld method using Topas-Academic v.4 software package.[54] Successive difference Fourier map calculations allowed the determination of one partially occupied O atom belonging to the water molecule located within the channels of the structure. Final Rietveld refinement converged with acceptable agreement factors of $R_p$ = 8.7 and $R_{wp}$ = 11.8. Details of Rietveld refinement along with the crystallographic parameters and crystal structure scheme for Ca-BDC-*tric* are available in the Supporting Information.

The syntheses yielding products containing a mixture of Ca-BDC-*orth* and Ca-BDC-*tric* were quantified for both phases. Quantification was performed on XRD pattern data recorded from 5 to 35° 2$\theta$ with the step of 0.016° by Rietveld procedure. First, full profile was refined using the ninth order Chebychev polynom for background refinement and PseudoVoigtVII function for peak shape refinement. After inclusion of CIF data for Ca-BDC-*orth* and Ca-BDC-*tric* phases, additional parameters were refined (scale factor, zero error, unit cell parameters, crystal sizes, and preferential orientation for Ca-BDC-*orth* using level 4 spherical harmonics). Rietveld quantification results for individual products are available in Supporting Information.

Morphologies and size of the crystals of obtained phases were observed by scanning electron microscopy measurements (SEM) on Zeiss Supra 3VP field-emission gun (FEG) microscope. Thermogravimetric (TG/DTG) analyses were performed on a SDT 2960 Thermal Analysis System (TA Instruments, Inc.). The measurement was carried out in static air with the heating rate of 10 °C/min. Fourier-transform infrared (FT-IR) measurements were performed on a PerkinElmer Spectrum One FTIR spectrometer with resolution of 1 $cm^{-1}$ from self-supporting KBr pellets. The specific surface area of the materials were determined by BET method based on the argon sorption measurements performed on an IMI-100 gas sorption analyzer (Hiden Isochema, Inc.) at 87 K in the range of relative pressures from $10^{-6}$ to 1. As-prepared pure Ca-BDC-*orth* and Ca-BDC-*tric* were degassed at 150 °C for 4 h prior to the measurements.

**Synthesis.** Two conformations of Ca(BDC)(DMF)($H_2O$) with different crystal symmetries were synthesized solvothermally by tuning the amount of added triethylamine and the temperature of crystallization.

Pure orthorhombic Ca(BDC)(DMF)($H_2O$), already reported by Liang et al.[50] (in further text denoted as Ca-BDC-*orth*), was formed by using the following procedure: 0.26 g (1 mmol) of $Ca(NO_3)_2{\cdot}6H_2O$ (99%, Sigma-Aldrich) was dissolved in 2 mL of demineralized water, and 0.18 g of terephthalic acid (95% BDC, Alfa Aesar) in a mixture of 8 mL (100 mmol) of *N*,*N*′-dimethylformamide (99% DMF, Aldrich) and 0.58 mL (1.63 mmol) of triethylamine (99% TEA, Aldrich). Two solutions were combined and solvothermally treated under autogenous pressure in a glass vessel at 150 °C for 24 h.

Pure triclinic Ca(BDC)(DMF)($H_2O$) (NICS-8), whose structure is reported here for the first time (in further text denoted as Ca-BDC-*tric*), was formed using identical synthesis procedure as for the synthesis of orthorhombic phase, only the solvothermal treatment was performed at 80 °C for 24 h.

For the purpose of phase formation studies three synthesis parameters were varied: TEA/$Ca^{2+}$ molar ratio (0−1.63), temperature



DOI: 10.1021/cg501273b
*Cryst. Growth Des.* 2015, 15, 617−624

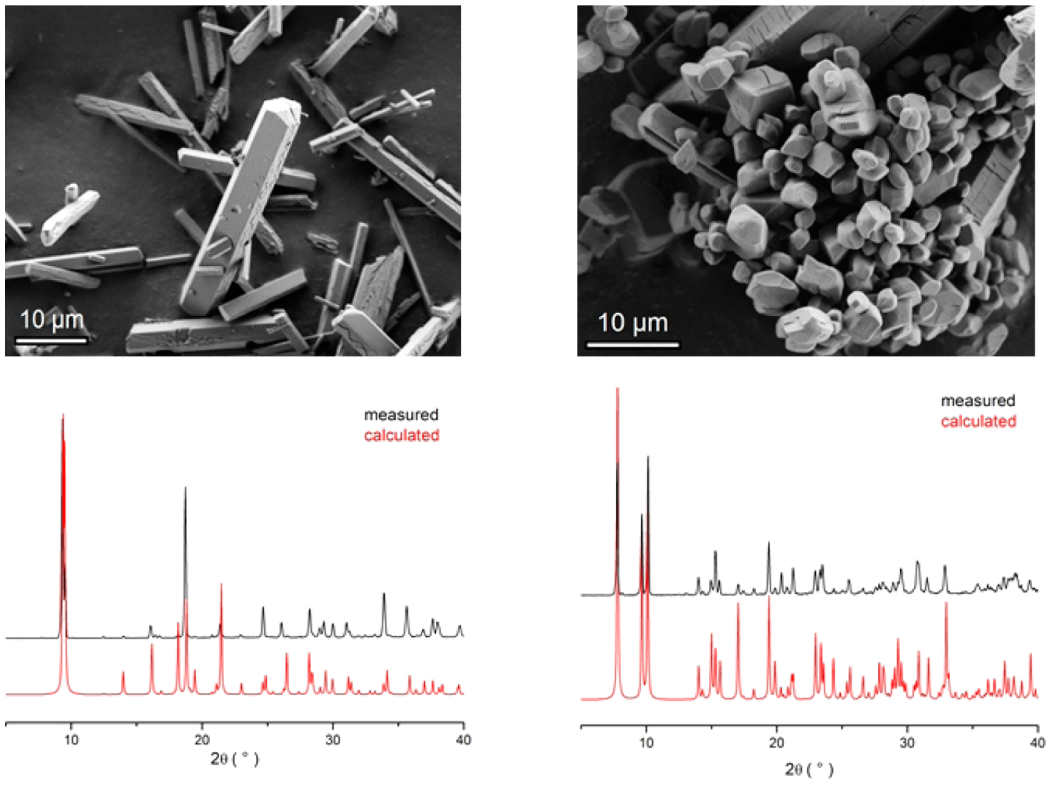


**Figure 2.** SEM micrographs of (a) Ca-BDC-*orth* and (b) Ca-BDC-*tric* phases with corresponding measured and calculated XRD patterns.

of crystallization (60−150 °C), and time of crystallization (24−72 h). All parameters were varied using two different $Ca^{2+}$ precursors: $Ca(NO_3)_2{\cdot}6H_2O$ and $CaCl_2{\cdot}4H_2O$. For monitoring the crystallization processes, the reaction mixtures with TEA/$Ca^{2+}$ molar ratios of 0, 0.3, and 1 were transferred into the preheated oven at 150 °C, respectively. The reactions were stopped at specified times by immediate cooling of the vessels under tapped water. The products were recovered by filtration without washing, dried at room temperature, and prepared for the XRD measurements.

## RESULTS AND DISCUSSION

**Crystal Structure Description and Structural Characterization.** Ca-BDC-*orth* and Ca-BDC-*tric* phases with formula $Ca(BDC)(DMF)(H_2O)$ possess the same topology, which was already described previously for orthorhombic phase,[49,50] but in order to discuss the differences in structural features, it will be briefly described again. The structures consist of zigzag chains of edge-sharing $CaO_8$ polyhedra with distorted bicapped prism geometry. Chains are linked with BDC ligands in two directions generating extended 3-dimensional framework with rhombic-shaped channels. Two bridging and four chelating O atoms belong to carboxylate groups of BDC ligands, whereas two additional O atoms coordinated to $Ca^{2+}$ belong to one water molecule and one DMF molecule, respectively. Main difference between Ca-BDC-*orth* and Ca-BDC-*tric* conformations lie in the orientation of the coordinated DMF molecule. Because of the partial delocalization of the C═O double bond, the DMF molecule tends to be planar, and three C atoms, which are bonded to N atom, can describe an imaginary plane. In orthorhombic phase, this plane is perpendicular to the direction of the channel, whereas in the case of triclinic phase it is approximately parallel in respect to the channel direction (Figure 1). Such orientation of DMF molecule causes complete blocking of the channels in the case of Ca-BDC-*orth* and making them inaccessible for any other guest molecules to adsorb. However, almost parallel plane-to-channel DMF orientation in Ca-BDC-*tric* provides some available space within the channels, resulting in partial occupation of the channels with the adsorbed water molecule.

Slight structural differences between the two conformations are evidently reflected in the results of some basic characterization methods. Ca-BDC-*orth* crystallizes in rod-like crystals with the size up to 50 μm, whereas Ca-BDC-*tric* is formed in the shape of prismatic crystals with the size of a few micrometers. Figure 2 shows SEM micrographs of both phases with corresponding XRD patterns.

The dynamics of structural changes during the heating process was already discussed in detail for Ca-BDC-*orth* phase.[49] However, the thermogravimetric analysis (Figure 3) shows notable differences between orthorhombic and triclinic phases in weight loss processes during the heating, particularly in the temperature range up to 100 °C. Ca-BDC-tric material contains ca. 5 wt % of surface water indicated by the weight loss gained up to 50 °C, whereas in the case of Ca-BDC-*orth* the weight loss in this temperature range is negligible. The weight losses in the second step between 80 and 120 °C are 13.0% and 16.3% for Ca-BDC-*orth* and Ca-BDC-*tric*, respectively. Weight loss in this step is not the consequence of the removal of only coordinated water but also partial removal of structural DMF, as it was shown for Ca-BDC-*orth* structure.[49] A similar process is expected to take place in the case of the triclinic phase. An approximately 3 wt % bigger weight change in the case of Ca-BDC-*tric* compared to Ca-BDC-*orth* can be attributed to the presence of a water molecule adsorbed within the channels of the triclinic phase with the occupancy of 1/2 per unit cell. This matches well with the Rietveld structure refinement results. Remaining DMF is removed from the materials up to 400 °C


DOI: 10.1021/cg501273b
*Cryst. Growth Des.* 2015, 15, 617−624

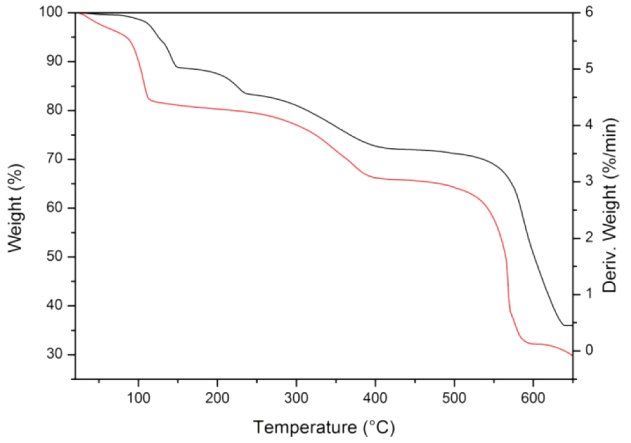


**Figure 3.** Thermogravimetric curves of Ca-BDC-*orth* (black line) and Ca-BDC-*tric* (red line) materials.

followed by final decomposition of Ca-BDC frameworks up to 600 °C in both cases.

Similar differences between two conformations of Ca-terephthalate structure can be observed in FT-IR spectra as well. Figure 4 shows FT-IR spectra of Ca-BDC-*orth* and Ca-BDC-*tric* materials in the range from 4000 to 2400 $cm^{-1}$. Both show broad bands with the peaks at 3360 $cm^{-1}$ due to the presence of surface water, and two extensively overlapped bands at 3510 and 3280 $cm^{-1}$, which can be assigned to the asymmetric and symmetric stretching of coordinated water molecules, respectively. The FT-IR spectrum of Ca-BDC-*tric* shows an additional overlapped band at 3465 $cm^{-1}$, which is not visible in spectra of Ca-BDC-*orth*, indicating the presence of water in another environment (adsorbed water) in Ca-BDC-*tric* material.

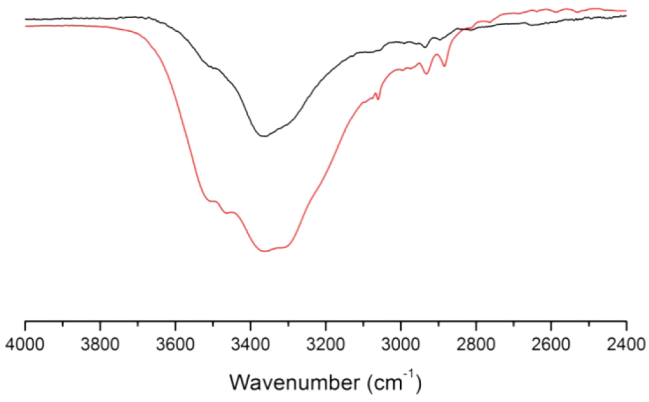


**Figure 4.** FT-IR spectra of Ca-BDC-*orth* (black line) and Ca-BDC-*tric* (red line) materials.

Different orientation of DMF methyl groups located within the channels of Ca-BDC-*orth* and Ca-BDC-*tric* structures also causes differences in the accessibility for gas molecules, which is reflected in the results of sorption analysis (Figure 5). For better evaluation of ultramicropore openings within the materials, Ar-based isotherms were measured. While Ca-BDC-*orth* does not show any notable uptake for argon and seems to be nonporous ($S_{BET}$ is not measurable), Ca-BDC-*tric* apparently has more accessible channels ($S_{BET}$ = 91 $m^2/g$), which is in agreement with the above-described structural findings. Continuous increase of the Ar uptake in the broad relative pressure range (from 0.1 to 1) in the case of Ca-BDC-*tric* material is most probably the consequence of slight cracking of the crystals during the degas process at 150 °C and thus the formation of mesopore voids.

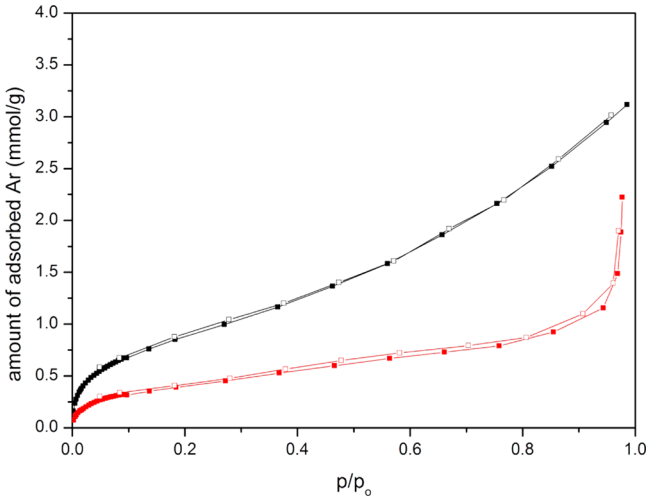


**Figure 5.** Ar sorption isotherm of Ca-BDC-*orth* (red line) and Ca-BDC-*tric* (black line) materials measured at 87 K. Adsorption points, full squares; desorption points, empty squares.

**Phase Formation and Crystallization Mechanism Study.** Ca(BDC)(DMF)($H_2O$) materials are formed in solvothermal conditions (using DMF/$H_2O$ mixture), and despite the very small structural differences between orthorhombic and triclinic conformations, the crystallization of individual phase can be controlled by changing certain synthesis parameters. The temperature of synthesis and the amount of triethylamine (TEA) added as a cosolvent turned out to have a crucial role in the formation of a certain phase. In order to understand how these two parameters influence the crystallization process, we performed a systematical study of phase formation at solvothermal conditions varying TEA/$Ca^{2+}$ molar ratios from 0 to 1.63 in the synthesis temperature range from 60 to 150 °C. Figure 6 shows the dependence of phase occurrence on TEA/$Ca^{2+}$ ratio and synthesis temperature after 1 and 3 days of crystallization, respectively. In the absence of triethylamine, the solvothermal reaction yields the mixture of triclinic and orthorhombic phases up to 130 °C after 1 day or up to 120 °C after 3 days of crystallization time. Only at higher temperatures, pure Ca-BDC-*orth* is formed. However, the presence of triethylamine apparently significantly changes the thermodynamics of the crystallization process. A small amount of cosolvent (TEA/$Ca^{2+}$ ratio of 0.33) directs the formation of pure Ca-BDC-*tric* at the synthesis temperatures below 90 °C. At higher temperatures the orthorhombic phase starts to appear and its yield is increasing with the increased temperature up to 140 °C, where triclinic phase is no longer present in the product. When TEA/$Ca^{2+}$ ratio is increased (0.63−1.30), much higher temperature of the synthesis is required for the Ca-BDC-*orth* phase to occur (120−130 °C). Interestingly, if the amount of TEA in the reaction mixture is increased even more (TEA/$Ca^{2+}$ ratio of 1.63), the orthorhombic conformation again starts to appear at lower temperatures (90 °C) yielding the pure Ca-BDC-*orth* product in the temperature range from 120 to 140 °C. In other words, Ca-BDC-*tric* is more stable in the system when the TEA/$Ca^{2+}$ ratio is within the range 0.6−1.3. It is also interesting to observe that the transformation process from the


DOI: 10.1021/cg501273b
*Cryst. Growth Des.* 2015, 15, 617−624

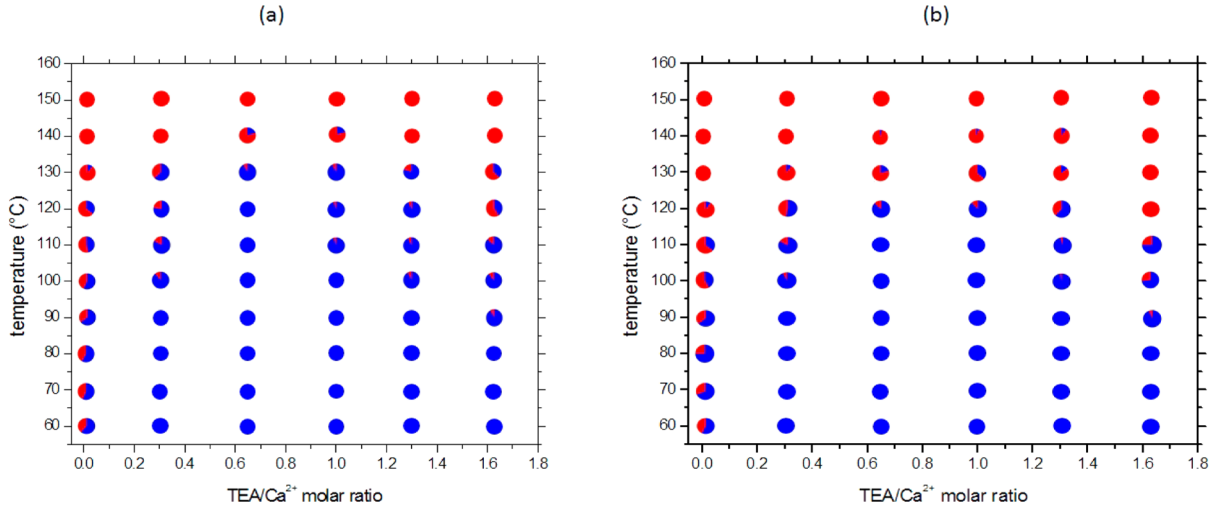


**Figure 6.** Phase diagram showing the dependence of TEA/$Ca^{2+}$ molar ratio using $Ca(NO_3)_2{\cdot}6H_2O$ as the precursor and the synthesis temperature on the occurrences of Ca-BDC-*orth* (red) and Ca-BDC-*tric* (blue) after (a) 24 h of crystallization and (b) 72 h of crystallization. Contributions of individual colors within circles are proportional to quantification results based on Rietveld analysis.

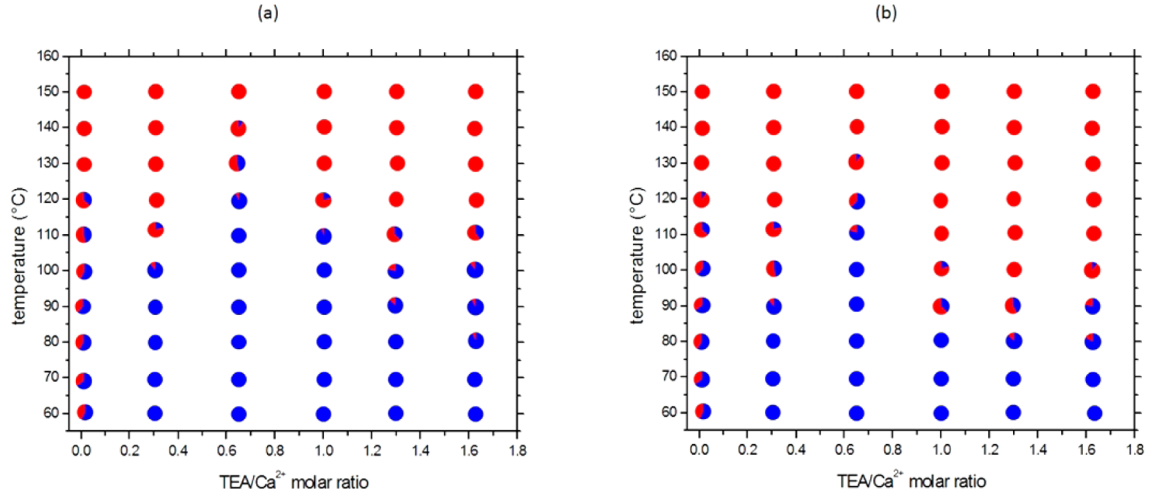


**Figure 7.** Phase diagram showing the dependence of TEA/$Ca^{2+}$ molar ratio using $CaCl_2{\cdot}4H_2O$ as the precursor and the synthesis temperature on the occurrences of Ca-BDC-*orth* (red) and Ca-BDC-*tric* (blue) after (a) 24 h of crystallization and (b) 72 h of crystallization. Contributions of individual colors within circles are proportional to quantification results based on Rietveld analysis.

pure triclinic to pure orthorhombic phases takes place over the much wider temperature range (90−130 °C) from the mixtures with TEA/$Ca^{2+}$ ratios of 0.3 and 1.63 compared to the transformation from the reaction mixtures with TEA/$Ca^{2+}$ ratios between 0.63 and 1.30. In the latter case the transformation occurs between 130 and 140 °C. Similar trends can be observed regardless of the time of crystallization; only after longer crystallization times slightly lower temperatures are required for the formation of orthorhombic phase. According to this investigation, Ca-BDC-*tric* and Ca-BDC-*orth* can be considered as low- and high-temperature conformations of $Ca(BDC)(DMF)(H_2O)$ structure, respectively.

Since counterions can also play a significant role in the kinetics and dynamics of crystallization processes, similar systematic investigation was also performed using $Ca(NO_3)_2{\cdot}6H_2O$ as a precursor instead of $CaCl_2{\cdot}4H_2O$. As can be seen from Figure 7, similar trends can be observed with the presence of $Cl^-$ or $NO_3^-$ ions; however, the Ca-BDC-*tric* to Ca-BDC-*orth* transformation occurs at somewhat lower temperatures (for approximately 10 °C), thus dynamics of crystal-to-crystal transformation seems to be slightly faster in the presence of $NO_3^-$ with respect to the system with $Cl^-$ ions.

In order to gain additional information on crystal growth of $Ca(BDC)(DMF)(H_2O)$ structures under solvothermal conditions, the crystallization process was monitored by XRD analysis. The crystallization from the reaction mixtures taking place at 150 °C was stopped at certain times of syntheses. Powder XRD analysis is exampled for the products obtained from the reaction mixture with the TEA/$Ca^{2+}$ molar ratio of 1, and their corresponding patterns are shown in Figure 8. When the aqueous solution of $Ca(NO_3)_2$ is combined with the solution of terephthalic acid in DMF, the exothermic reaction takes place instantly, yielding the product that corresponds to the already described material.[55−57] This structure is constructed of $Ca(BDC)(H_2O)_3$ chain-like units linked by hydrogen bonds into the pseudo three-dimensional structure, and it does not contain any DMF molecules. As it is indicated, this phase is transformed into the Ca-BDC-*tric* just after the 30 min of treatment at 150 °C. It must be taken into account that the actual temperature within the vessel after such period of


DOI: 10.1021/cg501273b
*Cryst. Growth Des.* 2015, 15, 617−624

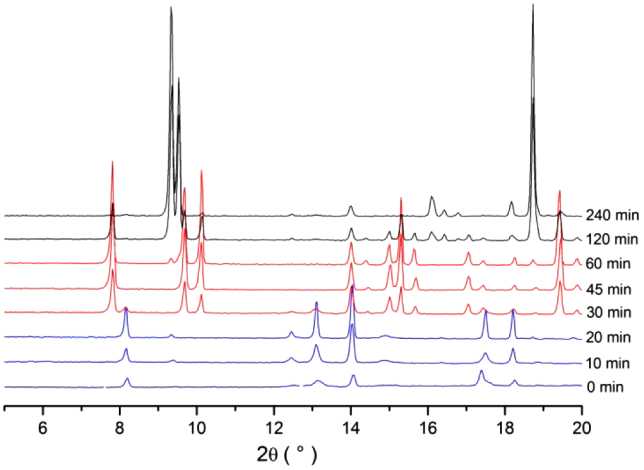


**Figure 8.** XRD powder patterns of the products obtained from reaction mixture with TEA/$Ca^{2+}$ = 1 molar ratio treated at 150 °C after the specified times of crystallization.

time is most probably still below 150 °C even though it was transferred in the preheated oven. After 1 h of solvothermal treatment, Ca-BDC-*orth* starts to appear and the content of triclinic phase starts to decrease with time. After 4 h, only orthorhombic conformation can be observed. This investigation shows that the kinetics of both crystal-to-crystal (CTC) transformations ($Ca(BDC)(H_2O)_3$ → Ca-BDC-*tric* and Ca-BDC-*tric* → Ca-BDC-*orth*) seem to be very fast when using TEA/$Ca^{2+}$ molar ratio of 1, and it is in agreement with the phase diagram. Similar experiments were performed for the products obtained from reaction mixture with TEA/$Ca^{2+}$ molar ratios 0 and 0.3, respectively (not shown). As expected, the formation of Ca-BDC-*orth* from reaction mixture with TEA/$Ca^{2+}$ of 0.3 undergoes the same CTC transformation processes as in the above-described system with higher amount of TEA within the initial mixture. However, in the TEA/$Ca^{2+}$ = 0.3 system, the second step (Ca-BDC-*tric* → Ca-BDC-*orth*) seems to be slower and expanded over the longer time period of solvothermal treatment. When solvothermal treatment is started from the reaction mixture in the absence of TEA, CTC transformation process is less controlled, leading to more or less simultaneous formation of both triclinic and orthorhombic conformations from the $Ca(BDC)(H_2O)_3$ structure. The mixture of phases is eventually transformed into the pure Ca-BDC-*orth* after 4 h of solvothermal treatment at 150 °C.

On the basis of our findings from phase occurrence studies, we can further discuss the mechanism of the Ca-BDC-*orth* crystallization process. The CTC transformations are schematically represented on Figure 9. When combining $Ca^{2+}$ cations in aqueous medium with terephthalate ions dissolved in DMF, these species are bonded instantly at room temperature forming $Ca(BDC)(H_2O)_3$. At this stage DMF is not yet involved in the crystallization process. However, only modestly elevated temperature is required for DMF to coordinate to $Ca^{2+}$ cations via the ligand exchange process with a water molecule, thus forming Ca-BDC-*tric*. When the temperature of crystallization is further elevated, the crystal symmetry of the formed $Ca(BDC)(DMF)(H_2O)$ is increased from triclinic to orthorhombic by slight rearrangement of benzene ring planes, change of DMF molecule orientation (rotation of methyl groups over the N atom center for approximately 60°), and

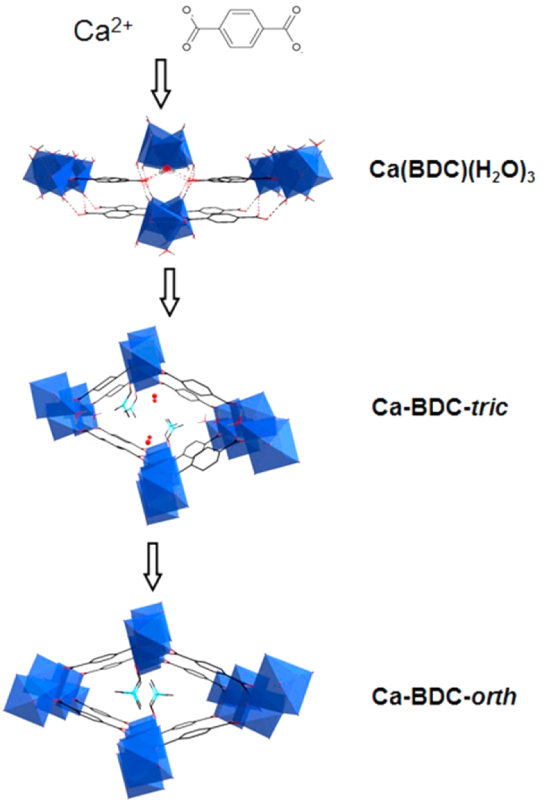


**Figure 9.** Scheme of crystal-to-crystal transformations from initial precursors into Ca-BDC-*orth* structure during the solvothermal treatment.

partial subsiding of the channels. This transformation seems to be the rate-determining step of the Ca-BDC-*orth* crystallization mechanism, and it is governed and tuned by the presence and the amount of triethylamine agent. Triethylamine is an organic base that is not directly involved in the framework formation, but its primary role in the crystallization process is obviously the tuning of pH value. Figure 10 shows how pH of the initial

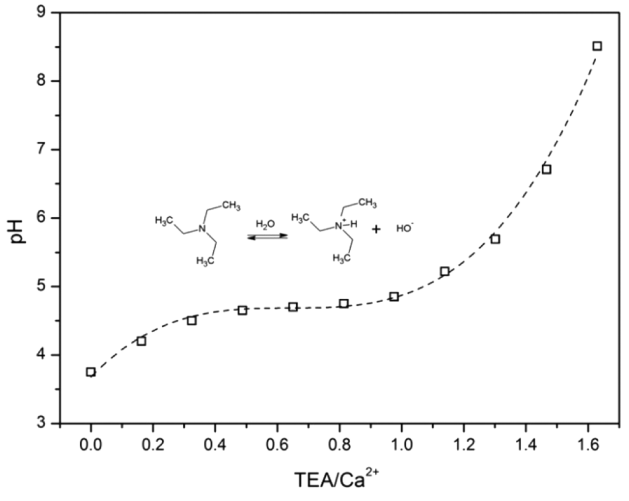


**Figure 10.** Dependence of pH vs TEA amount in the initial reaction mixture with the equilibrium reaction scheme of triethylamine dissociation. Squares show experimental pH values measured in the mixtures with corresponding amounts of TEA. Dotted line represents a trend-line drawn for easier interpretation of results.


DOI: 10.1021/cg501273b
*Cryst. Growth Des.* 2015, 15, 617−624

reaction mixture changes with the amount of added TEA agent. Ca-BDC-*tric* → Ca-BDC-*orth* transformation requires higher temperatures when pH of the initial reaction mixture is stabilized over the narrow buffer region between 4.5 and 5 ($TEA/Ca^{2+}$ = 0.63−1.30). When approximating to the equivalence point (pH > 6) and at pH below 4.0, the CTC transformation occurs at lower temperatures. It seems that triclinic phase is more stable in the narrow pH region around 4.5. In more acidic conditions (pH < 4) this process is less controllable, resulting in the simultaneous formation of both phases at lower temperatures and the formation of the pure orthorhombic phase at appropriately elevated temperatures. Similar phase occurrences can be observed when adjusting pH of the initial gel to 4.5 with aqueous solutions of NaOH or $NH_3$ instead of TEA and treating at the same synthesis conditions as described in the experimental section. This implies that structural dynamics of CTC transformation is not governed by the presence of species that are a result of the dissociation process ($Et_3NH^+$ or $OH^-$), but are most likely related to the thermodynamic state that is established at buffer conditions. In other words, Ca-BDC-tric is more stable at the solution conditions where the dissociation reaction of base is in equilibrium and the Gibbs free energy of the system is at its minimum. Thus, higher temperature is required for Ca-BDC-*tric* → Ca-BDC-*orth* transformation to occur at such conditions.

## CONCLUSIONS

$Ca(BDC)(DMF)(H_2O)$ structure crystallizes in solvothermal conditions from $H_2O$/DMF mixture in triclinic (Ca-BDC-*tric*) and orthorhombic (Ca-BDC-*orth*) conformations. Both structures possess the same square lattice net topology with rhombic-shaped channels, but they differ in the orientation of coordinated DMF molecules, which are located within the channels. This small structural difference is reflected in the accessibility of the pores. Openings in Ca-BDC-*orth* are completely blocked by structural DMF molecules, whereas Ca-BDC-*tric* shows some degree of permanent porosity. Study of the crystallization process showed that both phases are formed via crystal-to-crystal transformation from one-dimensional $Ca(BDC)(H_2O)_3$, which crystallizes instantly after mixing metal and ligand precursors in DMF/$H_2O$ solvent. Triclinic (metastable) phase is formed preferably at lower temperatures of solvothermal treatment, whereas for formation of orthorhombic phase higher temperature is required. We showed that dynamics of $Ca(BDC)(H_2O)_3$ → Ca-BDC-*tric* → Ca-BDC-*orth* transformations are mainly governed by the amount of the base agent (TEA), which is present in the reaction mixture, whereas the type of counterion has only minor influence on the dynamics of the transformation. When the $TEA/Ca^{2+}$ molar ratio in the starting reaction mixture is between 0.6 and 1.3, Ca-BDC-*tric* → Ca-BDC-*orth* occurs at 120 °C. If the $TEA/Ca^{2+}$ molar ratios are below and above that region, the transformation to orthorhombic phase starts at lower temperature (90 °C). The reaction mixture, having $TEA/Ca^{2+}$ ratio between 0.6 and 1.3, is within the buffer region of this solution system (pH ≈ 4.5), where dissociation reaction $Et_3N + H_2O \leftrightarrow Et_3NH^+ + OH^-$ reaches equilibrium. Since similar dynamics can be observed using other bases (NaOH or $NH_3$), stability of the triclinic phase seems to be related to the thermodynamic state at equilibrium conditions within the reaction system, which can be reached by tuning the pH of the solution. This investigation is a step forward toward understanding of the crystallization mechanisms of Ca-based MOF systems and could help to design the functional Ca-MOF systems with permanent porosity.

## ASSOCIATED CONTENT

### Supporting Information

Crystal structure scheme, refinement data with Rietveld plot, atomic coordinates, selected bonds and angles for Ca-BDC-*tric* (NICS-8), list of Ca-BDC-*orth* weight contributions within the products obtained after 1 and 3 days of crystallization at specified temperatures, and $TEA/Ca^{2+}$ molar ratios, based on the Rietveld quantification analyses. This material is available free of charge via the Internet at http://pubs.acs.org.

## AUTHOR INFORMATION

### Corresponding Author

*E-mail: matjaz.mazaj@ki.si. Phone: +38614760215. Fax: +38614760300.

### Author Contributions

The manuscript was written through contributions of all authors. All authors have given approval to the final version of the manuscript.

### Author Contributions

†These authors contributed equally to this work.

### Notes

The authors declare no competing financial interest.

## ACKNOWLEDGMENTS

This work was supported by the Slovenian Research Agency research program P1-0021.

## ABBREVIATIONS

MOFs, metal−organic frameworks; BDC, 1,4-benzenedicarboxylic acid; DMF, *N,N′*-dimethylformamide; TEA, triethylamine; NICS-8, National Institute of Chemistry Slovenia-8; SEM, scanning electron microscopy; FEG, field-emission gun; TG, thermogravimmetry; DTG, differential thermogravimetry; FT-IR, Fourier-transform infrared spectroscopy; CTC, crystal-to-crystal transformation; XRD, X-ray diffraction

## REFERENCES

(1) Liu, D.; Lu, K.; Poon, C.; Lin, W. *Inorg. Chem.* **2014**, *53*, 1916−1924.
(2) Gascon, J.; Corma, A.; Kapteijn, F.; Llabrés i Xamena, F. X. *ACS Catal.* **2014**, *4*, 361−378.
(3) Herm, Z. R.; Bloch, E. D.; Long, J. R. *Chem. Mater.* **2014**, *26*, 323−338.
(4) Wang, C.; Liu, D.; Lin, W. *J. Am. Chem. Soc.* **2013**, *135*, 13222−13234.
(5) Furukawa, H.; Cordova, K. E.; O'Keeffe, M.; Yaghi, O. M. *Science* **2013**, *341*, 1230444−1230444.
(6) Jiang, H.-L.; Makal, T. A.; Zhou, H.-C. *Coord. Chem. Rev.* **2013**, *257*, 2232−2249.
(7) Li, S.-L.; Xu, Q. *Energy Environ. Sci.* **2013**, *6*, 1656.
(8) Coronado, E.; Mínguez Espallargas, G. *Chem. Soc. Rev.* **2013**, *42*, 1525.
(9) Cook, T. R.; Zheng, Y.-R.; Stang, P. J. *Chem. Rev.* **2013**, *113*, 734−777.
(10) Khan, N. A.; Hasan, Z.; Jhung, S. H. *J. Hazard. Mater.* **2013**, *244−245*, 444−456.
(11) Tanh Jeazet, H. B.; Staudt, C.; Janiak, C. *Dalton Trans.* **2012**, *41*, 14003.
(12) Wang, J.-L.; Wang, C.; Lin, W. *ACS Catal.* **2012**, *2*, 2630−2640.
(13) Makal, T. A.; Li, J.-R.; Lu, W.; Zhou, H.-C. *Chem. Soc. Rev.* **2012**, *41*, 7761.



DOI: 10.1021/cg501273b
*Cryst. Growth Des.* 2015, 15, 617−624

(14) Masoomi, M. Y.; Morsali, A. *Coord. Chem. Rev.* **2012**, *256*, 2921−2943.
(15) Morozan, A.; Jaouen, F. *Energy Environ. Sci.* **2012**, *5*, 9269.
(16) Liu, J.; Thallapally, P. K.; McGrail, B. P.; Brown, D. R.; Liu, J. *Chem. Soc. Rev.* **2012**, *41*, 2308.
(17) Yoon, M.; Srirambalaji, R.; Kim, K. *Chem. Rev.* **2012**, *112*, 1196−1231.
(18) Kreno, L. E.; Leong, K.; Farha, O. K.; Allendorf, M.; Van Duyne, R. P.; Hupp, J. T. *Chem. Rev.* **2012**, *112*, 1105−1125.
(19) Wang, C.; Zhang, T.; Lin, W. *Chem. Rev.* **2012**, *112*, 1084−1104.
(20) Horcajada, P.; Gref, R.; Baati, T.; Allan, P. K.; Maurin, G.; Couvreur, P.; Férey, G.; Morris, R. E.; Serre, C. *Chem. Rev.* **2012**, *112*, 1232−1268.
(21) Li, J.-R.; Sculley, J.; Zhou, H.-C. *Chem. Rev.* **2012**, *112*, 869−932.
(22) Cui, Y.; Yue, Y.; Qian, G.; Chen, B. *Chem. Rev.* **2012**, *112*, 1126−1162.
(23) Li, C.-P.; Du, M. *Chem. Commun.* **2011**, *47*, 5958.
(24) Birsa Čelič, T.; Rangus, M.; Lázár, K.; Kaučič, V.; Zabukovec Logar, N. *Angew. Chem., Int. Ed.* **2012**, *51*, 12490−12494.
(25) Bu, X.-H.; Chen, W.; Hou, W.-F.; Du, M.; Zhang, R.-H.; Brisse, F. *Inorg. Chem.* **2002**, *41*, 3477−3482.
(26) Chen, Q.; Chang, Z.; Song, W.-C.; Song, H.; Song, H.-B.; Hu, T.-L.; Bu, X.-H. *Angew. Chem., Int. Ed.* **2013**, *52*, 11550−11553.
(27) Lu, Y.-L.; Wu, J.-Y.; Chan, M.-C.; Huang, S.-M.; Lin, C.-S.; Chiu, T.-W.; Liu, Y.-H.; Wen, Y.-S.; Ueng, C.-H.; Chin, T.-M.; Hung, C.-H.; Lu, K.-L. *Inorg. Chem.* **2006**, *45*, 2430−2437.
(28) He, R.; Song, H.; Wei, Z. *Inorg. Chim. Acta* **2010**, *363*, 2631−2636.
(29) Lan, Y.-Q.; Jiang, H.-L.; Li, S.-L.; Xu, Q. *Inorg. Chem.* **2012**, *51*, 7484−7491.
(30) Wang, F.-K.; Yang, S.-Y.; Huang, R.-B.; Zheng, L.-S.; Batten, S. R. *CrystEngComm* **2008**, *10*, 1211.
(31) Manos, M. J.; Moushi, E. E.; Papaefstathiou, G. S.; Tasiopoulos, A. J. *Cryst. Growth Des.* **2012**, *12*, 5471−5480.
(32) Sanz, R.; Martínez, F.; Orcajo, G.; Wojtas, L.; Briones, D. *Dalton Trans.* **2013**, *42*, 2392.
(33) Mazaj, M.; Birsa Čelič, T.; Mali, G.; Rangus, M.; Kaučič, V.; Zabukovec Logar, N. *Cryst. Growth Des.* **2013**, *13*, 3825−3834.
(34) Rosi, N. L.; Eddaoudi, M.; Kim, J.; O'Keeffe, M.; Yaghi, O. M. *CrystEngComm* **2002**, *4*, 401.
(35) Fang, Q.; Zhu, G.; Xue, M.; Wang, Z.; Sun, J.; Qiu, S. *Cryst. Growth Des.* **2008**, *8*, 319−329.
(36) Yaghi, O. M.; Li, G.; Li, H. *Chem. Mater.* **1997**, *9*, 1074−1076.
(37) Tian, Y.-Q.; Cai, C.-X.; Ji, Y.; You, X.-Z.; Peng, S.-M.; Lee, G.-H. *Angew. Chem., Int. Ed.* **2002**, *41*, 1384−1386.
(38) Zhang, X.-M.; Chen, X.-M. *Eur. J. Inorg. Chem.* **2003**, *2003*, 413−417.
(39) Yaghi, O. M.; Davis, C. E.; Li, G.; Li, H. *J. Am. Chem. Soc.* **1997**, *119*, 2861−2868.
(40) Wu, G.; Shi, X.; Fang, Q.; Tian, G.; Wang, L.; Zhu, G.; Addison, A. W.; Wei, Y.; Qiu, S. *Inorg. Chem. Commun.* **2003**, *6*, 402−404.
(41) Fang, Q.; Zhu, G.; Xue, M.; Sun, J.; Tian, G.; Wu, G.; Qiu, S. *Dalton Trans.* **2004**, 2202.
(42) Almeida Paz, F. A.; Klinowski, J. *J. Solid State Chem.* **2004**, *177*, 3423−3432.
(43) Gómez-Lor, B.; Gutiérrez-Puebla, E.; Iglesias, M.; Monge, M. A.; Ruiz-Valero, C.; Snejko, N. *Chem. Mater.* **2005**, *17*, 2568−2573.
(44) Fang, Q.; Zhu, G.; Xue, M.; Sun, J.; Sun, F.; Qiu, S. *Inorg. Chem.* **2006**, *45*, 3582−3587.
(45) Du, P.; Yang, Y.; Yang, J.; Liu, Y.-Y.; Kan, W.-Q.; Ma, J.-F. *CrystEngComm* **2013**, *15*, 6986.
(46) Senkovska, I.; Kaskel, S. *Eur. J. Inorg. Chem.* **2006**, *2006*, 4564−4569.
(47) Rood, J. A.; Boggess, W. C.; Noll, B. C.; Henderson, K. W. *J. Am. Chem. Soc.* **2007**, *129*, 13675−13682.
(48) Liu, H.-K.; Tsao, T.-H.; Zhang, Y.-T.; Lin, C.-H. *CrystEngComm* **2009**, *11*, 1462.
(49) Mazaj, M.; Mali, G.; Rangus, M.; Žunkovič, E.; Kaučič, V.; Zabukovec Logar, N. *J. Phys. Chem. C* **2013**, *117*, 7552−7564.
(50) Liang, P.-C.; Liu, H.-K.; Yeh, C.-T.; Lin, C.-H.; Zima, V. *Cryst. Growth Des.* **2011**, *11*, 699−708.
(51) Boultif, A.; Louër, D. *J. Appl. Crystallogr.* **2004**, *37*, 724−731.
(52) Le Bail, A.; Duroy, H.; Fourquet, J. L. *Mater. Res. Bull.* **1988**, *23*, 447−452.
(53) Altomare, A.; Camalli, M.; Cuocci, C.; Giacovazzo, C.; Moliterni, A.; Rizzi, R. *J. Appl. Crystallogr.* **2009**, *42*, 1197−1202.
(54) Coelho, A. Topas-Academic, Brisbane, Australia, 2007.
(55) Groeneman, R. H.; Atwood, J. L. *Cryst. Eng.* **1999**, *2*, 241−249.
(56) Matsuzaki, T.; Iitaka, Y. *Acta Crystallogr., Sect. B: Struct. Crystallogr. Cryst. Chem.* **1972**, *28*, 1977−1981.
(57) Dale, S. H.; Elsegood, M. R. J. *Acta Crystallogr., Sect. E: Struct. Rep. Online* **2003**, *59*, m586−m587.


DOI: 10.1021/cg501273b
*Cryst. Growth Des.* 2015, 15, 617−624